J Therm Anal Calorim (2014) 115:1119–1125
DOI 10.1007/s10973-013-3438-z

The study of thermal decomposition kinetics of zinc oxide formation from zinc oxalate dihydrate

Chengcheng Hu · Jie Mi · Suli Shang · Ju Shangguan

Received: 29 May 2013 / Accepted: 24 September 2013 / Published online: 22 October 2013

Abstract This study is devoted to the thermal decomposition of $ZnC_2O_4{\cdot}2H_2O$, which was synthesized by solid-state reaction using $C_2H_2O_4{\cdot}2H_2O$ and $Zn(CH_3COO)_2{\cdot}2H_2O$ as raw materials. The initial samples and the final solid thermal decomposition products were characterized by Fourier transform infrared and X-ray diffraction. The particle size of the products was observed by transmission electron microscopy. The thermal decomposition behavior was investigated by thermogravimetry, derivative thermogravimetric and differential thermal analysis. Experimental results show that the thermal decomposition reaction includes two stages: dehydration and decomposition, with nanostructured ZnO as the final solid product. The Ozawa integral method along with Coats–Redfern integral method was used to determine the kinetic model and kinetic parameters of the second thermal decomposition stage of $ZnC_2O_4{\cdot}2H_2O$. After calculation and comparison, the decomposition conforms to the nucleation and growth model and the physical interpretation is summarized. The activation energy and the kinetic mechanism function are determined to be 119.7 kJ mol^{-1} and $G(\alpha) = -\ln(1-\alpha)^{1/2}$, respectively.

Keywords Solid-state reaction · Thermal decomposition kinetics · Ozawa integral method · Coats–Redfern integral method · Nanostructured zinc oxide

C. Hu · J. Mi (✉) · S. Shang · J. Shangguan
Key Laboratory of Coal Science and Technology of Ministry of Education and Shanxi Province, Taiyuan University of Technology, Taiyuan 030024, People's Republic of China
e-mail: renyp080101@163.com

Introduction

Sulfur compounds (mainly as H_2S and COS) are the most abundant impurity in coal-derived synthesis gas (syngas) [1]. These species must be removed from the syngas prior to its utilization due to their negative effects on environment and chemical processing. Zinc oxide (ZnO) is known to be used as a highly efficient desulfurizer of coal-derived fuel gas and chemically synthesized gases [2–4] since it can reduce the concentration of H_2S to a few parts per million [5, 6]. Till now, many methods have been developed to synthesize nanostructured ZnO including direct precipitation [7], vapor–liquid–solid process [8], vapor phase growth [9], homogeneous precipitation [10], etc. However, thermal decomposition is one of essential steps for preparation of ZnO from different precursors.

Metal oxalate hydrates can be dehydrated and decomposed by heating to give the corresponding metal oxides, carbon monoxide, carbon dioxide, and water [11, 12]. Hence, metal oxalate hydrates have been exploited as precursors for preparing oxides by solid-state reaction methods [12–14]. Even if the thermal decomposition of $ZnC_2O_4{\cdot}2H_2O$ has been the subject of several studies [12, 15, 16], the mechanism and reaction kinetics of this transformation remains poorly understood.

Kinetic analysis of decomposition processes can be profitably of great importance to the understanding of behavior of intermediate products and products of thermal decomposition [17]. Number of analytical methods were developed in order to determine kinetic parameters for decomposition processes [18–20]. In fact, many of the present available kinetic methods differ from each other just due to their respective different approximations of the temperature-containing integral [21]. The experimental

kinetic data were usually analyzed using integral methods because of their inherent advantages [22].

In this paper, $ZnC_2O_4{\cdot}2H_2O$ was prepared and the thermal decomposition was investigated by means of both an experimental study and a numerical calculation. Two popular methods including those of Ozawa [23, 24] integral method and Coats and Redfern [25] integral method were applied to determine the kinetic model and the kinetic parameters of the second decomposition process of $ZnC_2O_4{\cdot}2H_2O$. The results will provide a theoretical basis for accurate design and preparation of ZnO-based desulfurization sorbents.

Experimental

Reagent and instrument

$Zn(CH_3COO)_2{\cdot}2H_2O$ (analytical-grade product, Tianjin Fengchuan Chemical Reagent Science and Technology Co. Ltd., China); $C_2H_2O_4{\cdot}2H_2O$ (analytical-grade product, Tianjin Fengchuan Chemical Reagent Science and Technology Co. Ltd., China); QM-3SP2 planetary ball mill (made in Nanjing, China).

Preparation

$ZnC_2O_4{\cdot}2H_2O$ was prepared by solid-state reaction from $C_2H_2O_4{\cdot}2H_2O$ and $Zn(CH_3COO)_2{\cdot}2H_2O$. Starting materials were thoroughly mixed with an agate mortar and pestle at a molar ratio of 1.0. The powder mechanical mixture was homogenized in a planetary ball mill for 2 h, and then dried in an oven at 80 °C for about 12 h.

Characterization

Spectroscopic properties were evaluated by a Fourier transform infrared (FTIR) spectrometer SHIMADZU FTIR-8400s, in the range of 4,000–400 cm^{-1} at room temperature. In the spectra, the transmittance was represented versus wavenumber (cm^{-1}).

The thermal properties were examined by German NETZSCH-STA409C thermal analyzer. A series of non-isothermal tests of $ZnC_2O_4{\cdot}2H_2O$ was carried out in a dynamic (40 mL min^{-1}) atmosphere of nitrogen from room temperature up to 600 °C at different heating rates of 5, 10, 15, and 20 °C min^{-1}. The sample mass used was about 10.0 mg.

The $ZnC_2O_4{\cdot}2H_2O$ and solid products of thermal decomposition were characterized by X-ray diffraction (XRD) using a Rigaku D/max-2500 equipped with graphite monochromatized Cu Kα radiation source ($\lambda = 1.5418$ Å) operating at 40 kV and 100 mA.

The particle size of the decomposition products was observed by transmission electron microscopy (TEM) (JEOL, JEM-1011) working at 100 kV with a point resolution of 0.3 nm.

Results and discussion

Thermal analyses of $ZnC_2O_4{\cdot}2H_2O$

Typical thermogravimetry (TG)–derivative thermogravimetric (DTG)/differential thermal analysis (DTA) curves of $ZnC_2O_4{\cdot}2H_2O$ at heating rate of 10 °C min^{-1} in nitrogen atmosphere are shown in Fig. 1. As shown by the TG curves, $ZnC_2O_4{\cdot}2H_2O$ has two mass loss stages. The first mass loss appears from 90 to 171 °C, accompanied by a large endothermic DTA peak at 152 °C with a slight shoulder on its low-temperature side (at 130 °C). The calculated mass loss agrees with the evolution of 2 mol H_2O per mole of $ZnC_2O_4{\cdot}2H_2O$. The second mass loss of 37.2 % (theoretical mass loss 38.03 %) appears between 300 and 400 °C, which is accompanied by a sharp endothermic peak at 402 °C, corresponding to the ZnC_2O_4 decomposition reaction. The total mass loss is 56.9 %, which is in good agreement with the calculated value of 57.1 % that can be calculated if it is assumed that the $ZnC_2O_4{\cdot}2H_2O$ is completely transformed into ZnO. The dehydration and decomposition correspond to the following reactions (1) [31] and (2) [16], respectively:

$$ZnC_2O_4 \cdot 2H_2O \rightarrow ZnC_2O_4 + 2H_2, \quad (1)$$

$$ZnC_2O_4 \rightarrow ZnO + CO_2 + CO. \quad (2)$$

XRD measurements

Typical XRD patterns of the initial sample and the products prepared at different thermal decomposition temperatures are shown in Fig. 2. The initial sample examined by XRD analysis is $ZnC_2O_4{\cdot}2H_2O$. The peak intensities derived from $ZnC_2O_4{\cdot}2H_2O$ decreased by raising the temperature to 270 °C, whereas those derived from the ZnC_2O_4 increased. At 300 °C, thermal decomposition products ZnO appear in the XRD patterns. The XRD patterns of the products obtained at temperatures of 330–390 °C show the peaks for only ZnO. By increasing the temperature, the crystallinity became more and more higher. The product obtained at 390 °C is in good agreement with the product, which was obtained at 420 °C. It is found that the thermal decomposition temperature occurs between 330 and 390 °C, which is consistent with the result obtained by TG.

FTIR analysis of $ZnC_2O_4{\cdot}2H_2O$

The FTIR spectra of $ZnC_2O_4{\cdot}2H_2O$ and the decomposition product are shown in Fig. 3. As shown in Fig. 3a, the

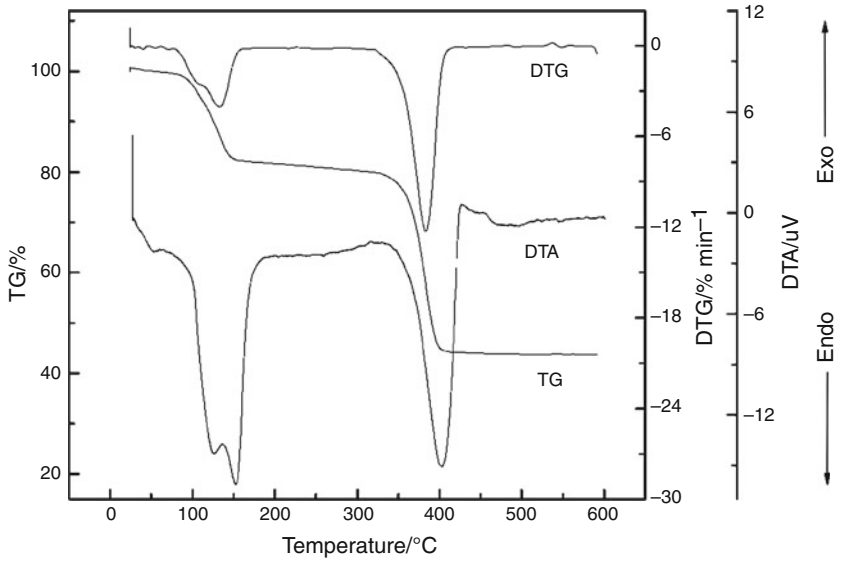

Fig. 1 TG–DTA/DTG curves for thermal decomposition of $ZnC_2O_4{\cdot}2H_2O$ in nitrogen ($\beta = 10$ °C min^{-1})

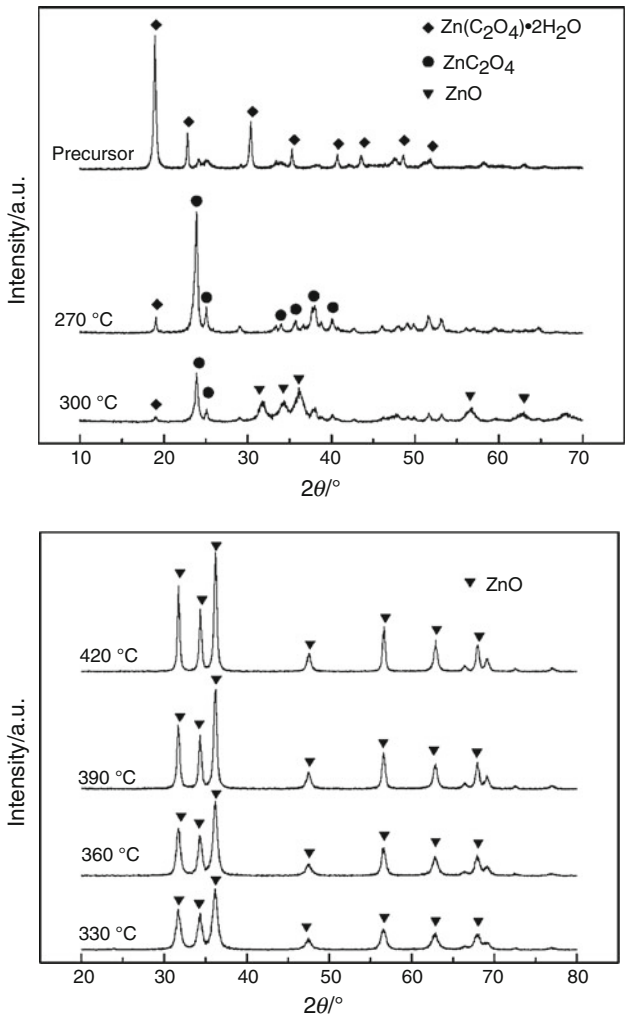

Fig. 2 XRD patterns of $ZnC_2O_4{\cdot}2H_2O$ and the products at different thermal decomposition temperatures

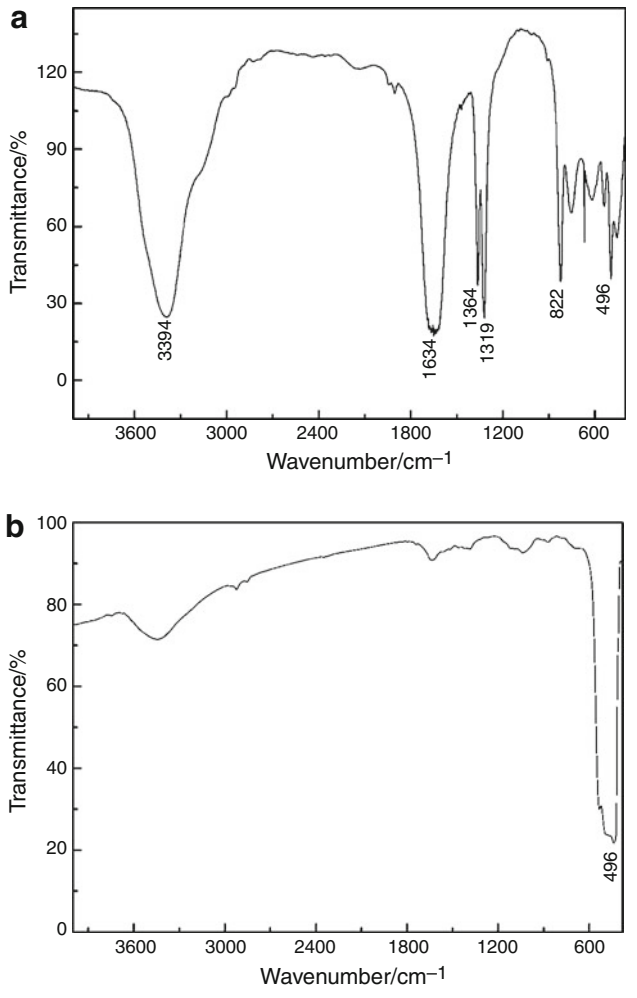

Fig. 3 FTIR spectra of $Zn(C_2O_4){\cdot}2H_2O$ and the decomposition product. **a** $Zn(C_2O_4){\cdot}2H_2O$, **b** the decomposition product

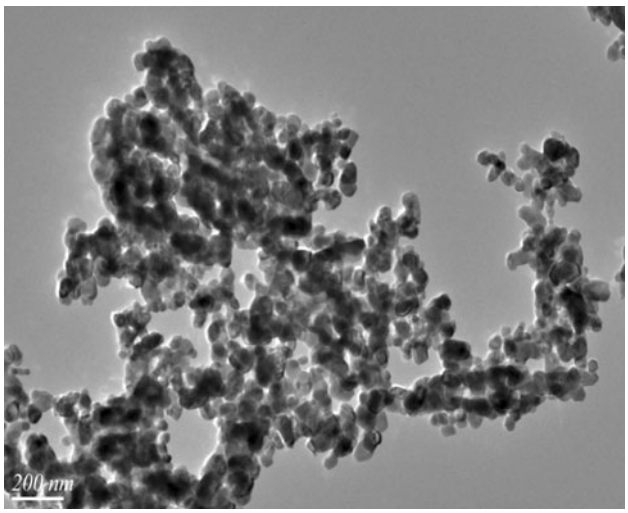

Fig. 4 Typical TEM photograph of the decomposition product

strong and broad band centered at about 3,394 cm^{-1} is assigned to stretching modes of hydrated water [26, 27], ν(O–H); This band is related to moisture in the sample. The strong band at 1,634 cm^{-1} is characteristic of C=O anti-symmetric stretching modes [26, 28], ν_{as}(C=O). The other peaks in this spectrum could be assigned as: the double band at 1,364 and 1,319 cm^{-1} is due to the O–C–O stretching modes [29], ν(O–C–O); the small band at 822 cm^{-1} is the C=C–O bending modes [29], δ(O–C=O); the band at 496 cm^{-1} is the Zn–O stretching modes [30], ν(Zn–O). From all the above, the initial sample is $ZnC_2O_4{\cdot}2H_2O$ without any other impurity. The FTIR spectra (Fig. 3b) of the final product indicate that ZnO is the only product, which is in good agreement with the result obtained by XRD.

TEM studies

TEM photograph of the decomposition product obtained at 390 °C is shown in Fig. 4. The ZnO nanoparticles are almost about 30–50 nm in size.

The effect of heating rate on the decomposition of $ZnC_2O_4{\cdot}2H_2O$

The DTA curves obtained at various heating rates (5, 10, 15, and 20 °C min^{-1}) for $ZnC_2O_4{\cdot}2H_2O$ are shown in Fig. 5. It is found that, with the increase of heating rate, the peak temperature of the first stage gradually shifts to the higher. For the second stage, the decomposition temperature shift to the higher linearly and the peaks become more and more sharp. These shifts in the first and second peak temperatures are shown in Fig. 6, and the decomposition peak is kinetically controlled.

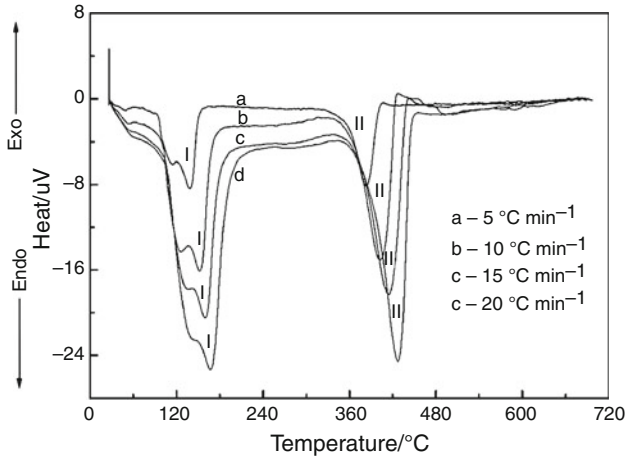

Fig. 5 DTA curves of thermal decomposition of $ZnC_2O_4{\cdot}2H_2O$ in nitrogen under different heating rates

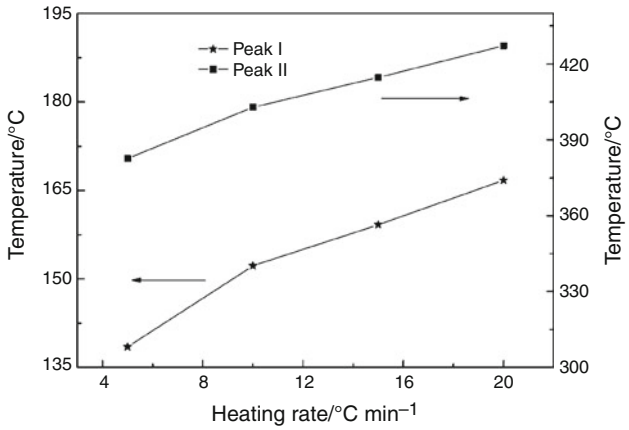

Fig. 6 Effect of the heating rate on the peak temperature of $ZnC_2O_4{\cdot}2H_2O$

Thermal decomposition kinetic of ZnC_2O_4

The Ozawa method is described with the following equation:

$$\log \beta = \log\left(\frac{AE}{RG(\alpha)}\right) - 2.315 - 0.4567\frac{E}{RT}. \quad (3)$$

The terms in Eq. (3) can be described as follows: $G(\alpha)$ stands for the conversion functional relationship, E is the

Table 1 The calculated data obtained from Fig. 6

β/°C min^{-1}	logβ	T_p/K	$1/T_p$
5	0.699	657.325	0.001521
10	1.000	677.048	0.001477
15	1.176	689.655	0.001450
20	1.301	699.791	0.001429

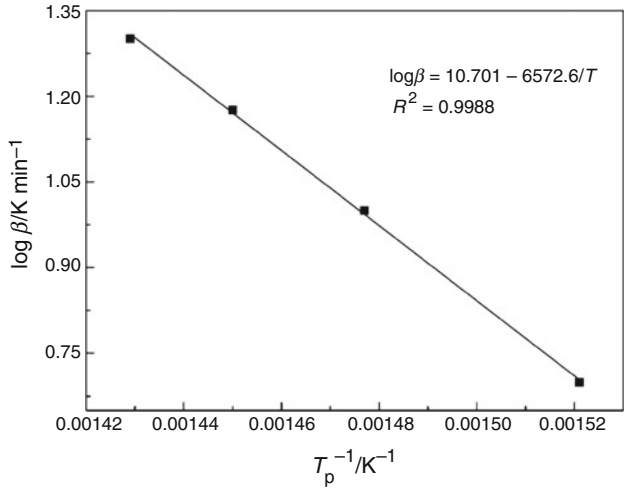

Fig. 7 The plot of logβ versus $1/T_p$ for ZnC_2O_4

activation energy, A is the pre-exponential factor, R is the universal gas constant, T is the absolute temperature, β is the heating rate, and $\alpha(0 < \alpha < 1)$ is the fractional conversion. The heating rate and the degree of conversion are defined as:

$$\beta = dT/dt, \tag{4}$$

$$\alpha = (m_0 - m)/(m_0 - m_f), \tag{5}$$

where m_0, m, and m_f refers to the initial, actual, and final mass of the sample.

The Ozawa method allows evaluating the dependence of the activation energy on the degree of conversion without the knowledge of the explicit form of $G(\alpha)$ [32, 33]. At the peak temperature, the degree of conversion α at different heating rates would be at a constant value [34], the reaction rate at a constant extent of conversion is only a function of the temperature. All the calculated data obtained from Fig. 6 (peak II) are summarized in Table 1.

The plot of logarithm of heating rates versus reciprocal of the absolute peak temperature for ZnC_2O_4 is described in Fig. 7. It could be found that the logβ against $1/T_p$ is straight lines with $R^2 = 0.9988$, which indicates that the mechanism of decomposition of ZnC_2O_4 is the first order [35]. The slope

Table 2 The data of temperature at different α values

α	0.1	0.2	0.3	0.4	0.5	0.6	0.7	0.8
T(K)	624.527	635.895	641.499	647.105	652.686	655.502	658.339	661.181

Table 3 $G(\alpha)$ integral kinetic equations for different mechanisms

No.	Function name	Mechanism	Symbols	Integral equation
1	Parabolic law	Diffusion, 1D	D_1	α^2
2	Valensi(Barrer) eqn.	Diffusion, 2D	D_2	$(1-\alpha)\ln(1-\alpha)+\alpha$
3	Ginstling–Broushtein eqn.	Diffusion, 3D (column symmetry)	D_3	$[1-(1-\alpha)^{1/3}]^2$
4	Jander eqn.	Diffusion, 3D (ball symmetry)	D_4	$(1-2\alpha/3)-(1-\alpha)^{2/3}$
5	Anti-Jander eqn.	Diffusion, 3D	D_5	$\{[1/(1-\alpha)]^{1/3}-1\}^2$
6	Zhuralev, Lesokin, and tempelmen eqn.	Diffusion, 3D	D_6	$[(1+\alpha)^{1/3}-1]^2$
7		Self-catalyzed reaction	A_u	$\ln[\alpha/(1-\alpha)]$
8–12	Avrami–Erofeev eqn.	N and G ($n = 1, 1.5, 2, 3, 4$)	A_n	$[-\ln(1-\alpha)]^{1/n}$
13		Shrinkage geometric shape (column symmetry)	R_1	$1-(1-\alpha)^{1/2}$
14		Shrinkage geometric shape (ball symmetry)	R_2	$1-(1-\alpha)^{1/3}$
15	Mampel power law		P_1	α
16	Mampel power law		P_2	$\alpha^{1/2}$
17	Mampel power law		P_3	$\alpha^{1/3}$
18	Mampel power law		P_4	$\alpha^{1/4}$
19	Second order	Chemical reaction (2nd order)	C_2	$(1-\alpha)^{-1}-1$
20	One and one-half order	Chemical reaction (1 and 1.5 order)	$C_{1/1.5}$	$(1-\alpha)^{-1/2}$
21				$1/(1-\alpha)$
22				$1/(1-\alpha)^2$

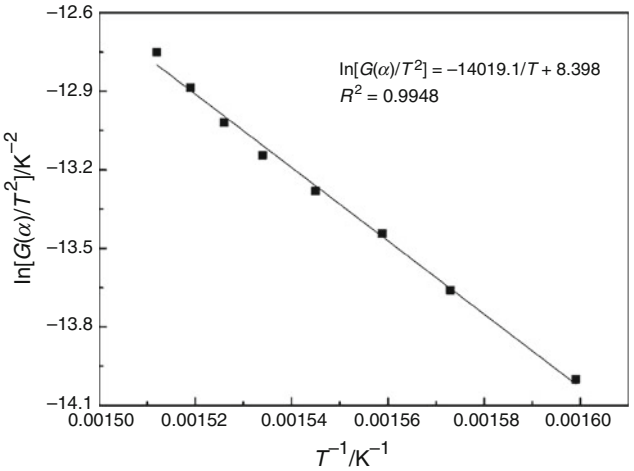

Fig. 8 The plot of $\ln[G(\alpha)/T^2]$ versus $1/T$ for ZnC_2O_4

of the line is equal to $-0.4567E_a/R$. Therefore, the activation energy (E_a) can be obtained from the slope of the graph. The calculated value of activation energy is 119.7 kJ mol^{-1} (theoretical value 80–250 kJ mol^{-1}) and the linear equation can be described as:

$$\log \beta = 10.701 - 6572.6/T. \quad (6)$$

The Coats–Redfern method is described with the following equation:

$$\ln\left[\frac{G(\alpha)}{T^2}\right] = \ln\left[\frac{AR}{\beta E}\right] - \frac{E}{RT}. \quad (7)$$

The terms in Eq. (7) have the same meaning with those in Eq. (3).

All the basic data of temperature at different α values obtained from TG to DTG (Fig. 1) are summarized in Table 2. The activation energy E_b can calculated from the linear equation of $\ln[G(\alpha)/T^2]$ versus $1/T$. The different forms of $G(\alpha)$ [36–40] are shown in Table 3. The most similar E_b obtained by comparing with E_a is 116.6 kJ mol^{-1}. The appropriate function $G(\alpha)$ corresponding to E_b is regarded as the optimum kinetic function. The plot of $\ln[G(\alpha)/T^2]$ versus $1/T$ for the ZnC_2O_4 is shown in Fig. 8.

After calculation, the kinetic mechanism function and linear equation could be shown as:

$$G(\alpha) = -\ln(1-\alpha)^{1/2}. \quad (8)$$

$$\ln\left[G(\alpha)/T^2\right] = -14019.1/T + 8.398. \quad (9)$$

It should be mentioned that, each measurement was performed a minimum of two times, but more typically three or four times, to ensure reproducibility. The decomposition conforms to the nucleation and growth model, and the physical interpretation is summarized as follows: The reaction starts at separated points on the crystal surface, where the lattice defects existed. The core of a new phase is formed by these adjacent decomposition products; afterward, the interface reaction of perinuclear moleculars occurs on the nucleus. The growth and extension of the new phase are accompanied by the disappearance of the old phase, until the whole solid phase has decomposed completely. The nucleus would be able to grow and expand quickly once it is formed, since the formation activation energy of the nucleus is larger than the growth activation energy [36].

Conclusions

The thermal decomposition of $ZnC_2O_4{\cdot}2H_2O$ has been studied by a series of experiment and calculation. Experimental results indicate that the thermal decomposition process includes two stages: dehydration and decomposition, with nanostructured ZnO as the final solid product. Much attention has been focused on the kinetics and mechanism of the second decomposition stage. After calculation and comparison, the decomposition conforms to the nucleation and growth model. The activation energy obtained from the DTA data by non-isothermal method proposed by Ozawa integral method is 119.7 kJ mol^{-1}. The kinetic mechanism function obtained by Coats–Redfern integral method and Ozawa integral method could be described by the following expression:

$$G(\alpha) = -\ln(1-\alpha)^{1/2}. \quad (10)$$

Acknowledgements This project was supported by the National Natural Science Foundation of China (51272170/21276172) and the Key Programs for Science and Technology Development of Shanxi Province under Contract (No. 20080322035).

References

1. Dolan MD, Ilyushechkin AY, McLennan KG, Nguyen T, Sharma SD. Glass-based processing of mixed-oxide desulfurization sorbents. Ind Eng Chem Res. 2009;48:10498–503.
2. Fan HL, Li YX, Li CH, Guo HX, Xie KC. The apparent kinetics of H_2S removal by zinc oxide in the presence of hydrogen. Fuel. 2002;81:91–6.
3. Novochinskii II, Song CS, Ma XL, Liu XS, Shore L, Lampert J, Farrauto RJ. Low-temperature H_2S removal from steam-containing gas mixtures with ZnO for fuel cell application. 1. ZnO particles and extrudates. Energy Fuels. 2004;18:576–83.
4. Yang HY, Sothen R, Cahela DR, Tatarchuk BJ. Breakthrough characteristics of reformate desulfurization using ZnO sorbents for logistic fuel cell power systems. Ind Eng Chem Res. 2008;47:10064–70.
5. Ling LX, Zhang RG, Han PD, Wang BJ. DFT study on the sulfurization mechanism during the desulfurization of H_2S on the ZnO desulfurizer. Fuel Process Technol. 2013;106:222–30.
6. Rodriguez JA, Maiti A. Adsorption and decomposition of H_2S on MgO(100), NiMgO(100), and ZnO(0001) surfaces: a first-principles density functional study. J Phys Chem B. 2000;104:3630–8.

7. Masuda Y, Kinoshita N, Koumoto K. Morphology control of ZnO crystalline particles in aqueous solution. Electrochim Acta. 2007;53:171–4.
8. Gao PX, Wang ZL. Nanopropeller arrays of zinc oxide. Appl Phys Lett. 2004;84:2883–5.
9. Sun XC, Zhang HZ, Xu J, Zhao Q, Wang RM, Yu DP. Shape controllable synthesis of ZnO nanorod arrays via vapor phase growth. Solid State Commun. 2004;129:803–7.
10. Liu Y, Zhou JE, Larbot A, Persin M. Preparation and characterization of nano-zinc oxide. J Mater Process Technol. 2007;189:379–83.
11. Raje N, Reddy AVR. Mechanistic aspects of thermal decomposition of thorium oxalate hexahydrate: a review. Thermochim Acta. 2010;505:53–8.
12. Suino A, Toyama S, Takesue M, Hayashi H, Smith RL Jr. Thermal analysis and mechanism of α-Zn_2SiO_4:Mn^{2+} formation from zinc oxalate dihydrate under hydrothermal conditions. Mater Chem Phys. 2013;137:1025–30.
13. Cong CJ, Hong JH, Liu QY, Liao L, Zhang KL. Synthesis, structure and ferromagnetic properties of Ni-doped ZnO nanparticles. Solid State Commun. 2006;138:511–5.
14. Peiteado M, Caballero AC, Makovec D. Phase evolution of $Zn_{1-x}Mn_xO$ system synthesized via oxalate precursors. J Eur Ceram Soc. 2007;27:3915–8.
15. Małecka B, Drozdz-Ciesla E, Małecki A. Mechanism and kinetics of thermal decomposition of zinc oxalate. Thermochim Acta. 2004;423:13–8.
16. Majumdar R, Sarkar P, Ray U, Roy MM. Secondary catalytic reactions during thermal decomposition of oxalates of zinc, nickel and iron(II). Thermochim Acta. 1999;335:43–53.
17. Findorakova L, Svoboda R. Kinetic analysis of the thermal decomposition of Zn(II) 2-chlorobenzoate complex with caffeine. Thermochim Acta. 2012;543:113–7.
18. Perejon A, Sanchez-Jimenez PE, Criado JM, Perez-Maqueda LA. Kinetic analysis of complex solid-state reactions. A new deconvolution procedure. J Phys Chem B. 2011;115:1780–91.
19. Svoboda R, Malek J. Applicability of Fraser–Suzuki function in kinetic analysis of complex crystallization processes. J Therm Anal Calorim. 2013;. doi:10.1007/s1097301224459.
20. Rocco JAFF, Lima JES, Frutuoso AG, Iha K, Ionashiro M, Matos JR, Suárez-Iha MEV. Thermal degradation of a composite solid propellant examined by DSC: kinetic study. J Therm Anal Calorim. 2004;75:551–7.
21. Liu NA, Fan WC, Dobashi R, Huang LS. Kinetic modeling of thermal decomposition of natural cellulosic materials in air atmosphere. J Anal Appl Pyrolysis. 2002;63:303–25.
22. Deng CJ, Cai JM, Liu RH. Kinetic analysis of solid-state reactions: evaluation of approximations to temperature integral and their applications. Solid State Sci. 2009;11:1375–9.
23. Ozawa T. A new method of analyzing thermogravimetric data. Bull Chem Soc Jpn. 1965;38:1881–6.
24. Ozawa T. Kinetic analysis of derivative curves in thermal analysis. J Therm Anal. 1970;2:301–24.
25. Coats AW, Redfern JP. Kinetic parameters from thermogravimetric data. Nature. 1964;201:68–9.
26. Angermann A, Töpfer J. Synthesis of nanocrystalline Mn–Zn ferrite powders through thermolysis of mixed oxalates. Ceram Int. 2011;37:995–1002.
27. Behnoudnia F, Dehghani H. Synthesis and characterization of novel three-dimensional-cauliflower-like nanostructure of lead(II) oxalate and its thermal decomposition for preparation of PbO. Inorg Chem Commun. 2012;24:32–9.
28. Frost RL, Weier ML. Thermal decomposition of humboldtine—a high resolution thermogravimetric and hot stage Raman spectroscopic study. J Therm Anal Calorim. 2004;75:277–91.
29. Gabal MA, Ata-Allah SS. Concerning the cation distribution in $MnFe_2O_4$ synthesized through the thermal decomposition of oxalates. J Phys Chem Solids. 2004;65:995–1003.
30. Yang L, Wang GZ, Tang CJ, Wang HQ, Zhang LD. Synthesis and photoluminescence of corn-like ZnO nanostructures under solvothermal-assisted heat treatment. Chem Phys Lett. 2005;409:337–41.
31. Dollimore D. The thermal decomposition of oxalates. A review. Thermochim Acta. 1987;117:331–63.
32. Wang QF, Wang L, Zhang XW, Mi ZT. Thermal stability and kinetic of decomposition of nitrated HTPB. J Hazard Mater. 2009;172:1659–64.
33. Salla JM, Morancho JM, Cadenato A, Ramis X. Non-isothermal degradation of a thermoset powder coating in inert and oxidant atmospheres. J Therm Anal Calorim. 2004;72:719–28.
34. Yi J, Zhao F, Xu S, Zhang L, Gao H, Hu R. Effects of pressure and TEGDN content on decomposition reaction mechanism and kinetics of DB gun propellant containing the mixed ester of TEGDN and NG. J Hazard Mater. 2009;165:853–9.
35. Sunitha M, Reghunadhan Nair CP, Krishnan K, Ninan KN. Kinetics of Alder-ene reaction of Tris(2-allylphenoxy)triphenoxycyclotriphosphazene and bismaleimides—a DSC study. Thermochim Acta. 2001;374:159–69.
36. Pan YX, Guan XY, Feng ZY, Li XY, Wu YS. A new method determining mechanism function of solid state reaction—the non-isothermal kinetic of dehydration of nickel(II) oxalate dihydrate in Solid State. Chin J Inorg Chem. 1999;15:247–51.
37. Gao X, Dollimore D. The thermal decomposition of oxalates. Part 26. A kinetic study of the thermal decomposition of manganese(I1) oxalate dihydrate. Thermochim Acta. 1993;215:47–63.
38. Turmanoval SCh, Genieva SD, Dimitrova AS, Vlaev LT. Non-isothermal degradation kinetics of filled with rise husk ash polypropene composites. Express Polym Lett. 2008;. doi:10.3144/expresspolymlett.
39. Noisong P, Danvirutai C. Kinetics and mechanism of thermal dehydration of $KMnPO_4{\cdot}H_2O$ in a nitrogen atmosphere. Ind Eng Chem Res. 2010;49:3146–51.
40. Galwey AK, Brown NE. Thermal decomposition of ionic solids. Netherlands: Elsevier; 1999.